RESEARCH REPORT 2012:07

A PIV Study of The Cooling Air Flow in An Electric Generator Model

by

Erwin Adi Hartono, Maxim Golubev, Pirooz Moradnia,
Valery Chernoray, Håkan Nilsson

Department of Applied Mechanics
CHALMERS UNIVERSITY OF TECHNOLOGY
Göteborg, Sweden, 2012

A PIV Study of The Cooling Air Flow in An Electric Generator Model

Erwin Adi Hartono, Maxim Golubev, Pirooz Moradnia, Valery Chernoray, Håkan Nilsson

Research report 2012:07
ISSN 1652-8549

Department of Applied Mechanics
Chalmers University of Technology
SE-412 96 Göteborg
Sweden
Telephone +46-(0)31-7721000

This document was typeset using LaTeX

Göteborg, Sweden, 2012

A PIV Study of The Cooling Air Flow in An Electric Generator Model

ERWIN ADI HARTONO, MAXIM GOLUBEV, PIROOZ MORADNIA, VALERY CHERNORAY, HÅKAN NILSSON

erwin-adi.hartono@chalmers.se
Department of Applied Mechanics
Chalmers University of Technology

Abstract

One factor that affects the performance of a hydro power generator is temperature. The efficiency, the electric resistance, the cables, the windings, etc, are temperature-dependent. These make controlling temperature rise in a generator of high importance in order to minimize hot spots and material failure. In order to tackle the problem air is used as a cooling fluid, which circulates through the stator and rotor in the generator.

A generator model has been specially designed to perform fluid flow measurement. 2D-2C PIV (Two Dimension - Two Component Particle Image Velocimetry) was used to measure the fluid velocity inside the stator channels. Stereo PIV (2D-3C) was used to measure fluid velocity outside of the stator body.

The results show that the tangential velocity component dominates the flow outside the stator. Inside the stator channels the fluid moves radially with a large recirculation region (almost half of the channel width) behind the coil. The flow structure inside the channels is shown to be independent of the rotor pole position.

Keywords: PIV, Air-Flow, Experimental, Hydro-Power, Generator

Acknowledgments

This report is an extended work of Erwin Adi Hartono's master thesis. We greatly acknowledge to Ångpanneföreningens Forskningsstiftelse for the funding, and VG Power for the feedback on the design.

Erwin Adi Hartono, Maxim Golubev, Pirooz Moradnia, Valery Chernoray, Håkan Nilsson
Gothenburg-Sweden
May 2012

Contents

Chapter 1

Introduction

1.1 Background

The importance of cooling in hydro-electric generators is high. This is because the main components of the generator, the cables and windings, are temperature-dependent. That is why the working temperature of the generator has to be controlled, in order to minimize hot-spots that can cause material failure, and also to increase efficiency of the generator itself.

1.2 Previous Studies

Hartono (2011) studied the airflow inside a generator model by measuring pressure in several interesting positions in the generator, e.g. around the coils and outside the channels. Figure 1.1 shows the schematic of the generator model.

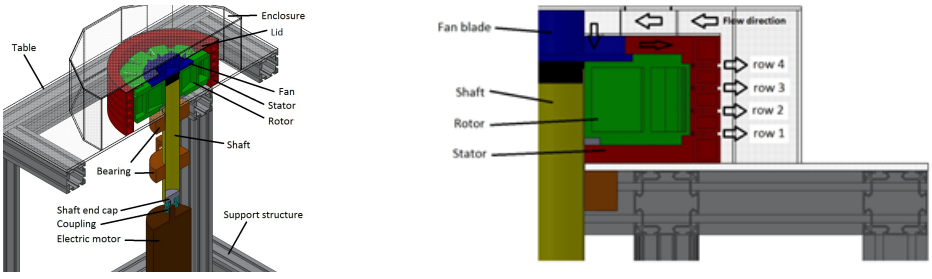

(a) 3D view of generator model

(b) 2D view of generator model with the flow direction and row numbering

Figure 1.1: Schematic of genearator model

Static pressure was measured inside the channels in order to study how the flow behaves at the coils, and total pressure was measured outside the channels to estimate the outlet mass flow distribution. The measurements showed that there were large recirculation bubbles inside the stator channels. The recirculation area consumes almost half of the channel width. This phenomenon occurred for different configurations of fan blades (short, medium and long) and stator channel baffles (straight and curved).

Moradnia et al. (2011) measured the air flow in an existing generator model at Uppsala University in Sweden. They measured the inlet and outlet velocity and also did a flow visualization at the inlet using a smoke pen. The measurement data was compared with numerical data. The comparison showed a relatively good quantitative agreement although there were geometrical dissimilarities between the rig and the computational domain.

Moradnia (2010) studied the air flow inside the Uppsala generator numerically. He used the frozen rotor concept, yielding steady results. Several geometrical modifications and turbulence models were studied. He concluded that the addition of baffles and fan blades increases the volume flow and reduce the recirculation regions inside the channels.

Lidell et al. (2001) studied the over-heating problem that was faced by Roxburgh's hydro power generator. They used a numerical approach and came up with a solution by redesigning the existing fan blade. The results showed that the re-designed blade gave 40% increase in pressure, 40 - 60% reduction in local viscous losses and 10% increase of local windage losses.

Previous study indicates that simple modification gives high impact in the performance of the generator cooling.

1.3 Purpose

The purpose of this work is to study, with great detail, air flow in the electric generator model. PIV was used to measure the velocity distribution of the air flow. The PIV measurements complement the previous pressure measurements.

The experimental data that was generated in this work yields a database for validation of numerical results.

1.4 Limitations

The studies in this work were limited to the short fan blades and two stator channel configurations. This particular fan was chosen because, according to the previous data, although the mass flow that was generated by the short fan was 20% lower than that of the medium size fan, we assumed that the short fan would be more beneficial in terms of fan losses.

Chapter 2

Method

PIV is the best method nowadays to indirectly measure the velocity field. The measurement region is seeded with tiny particles. A thin sheet of laser light with high frequency is used to light up the measurement region. The movement of the particles is captured with high speed camera. The velocity vectors are then obtained by calculating the displacement of the particles between two images.

Location of measurement are illustrated in figure 2.1. There are three main region that was studied. They were: inner region (1), outer region (2), and channel (3).

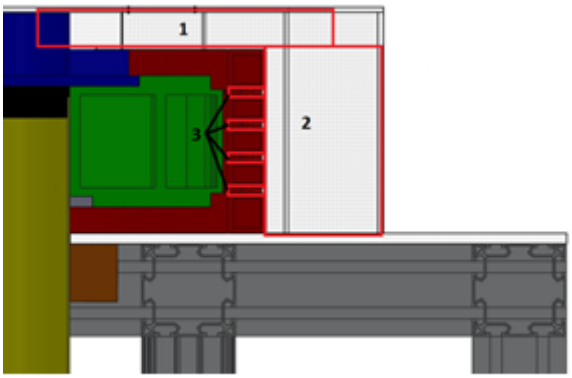

Figure 2.1: Locations of the measurement

A 2D-2C PIV configuration was used to measure the velocity field inside the stator channels and 2D-3C (stereo PIV) was used when measuring the velocity field outside the stator. Figure 2.2 shows a schematic of the 2D-2C and 2D-3C PIV setup.

The reason why different methods were used in the those two re-

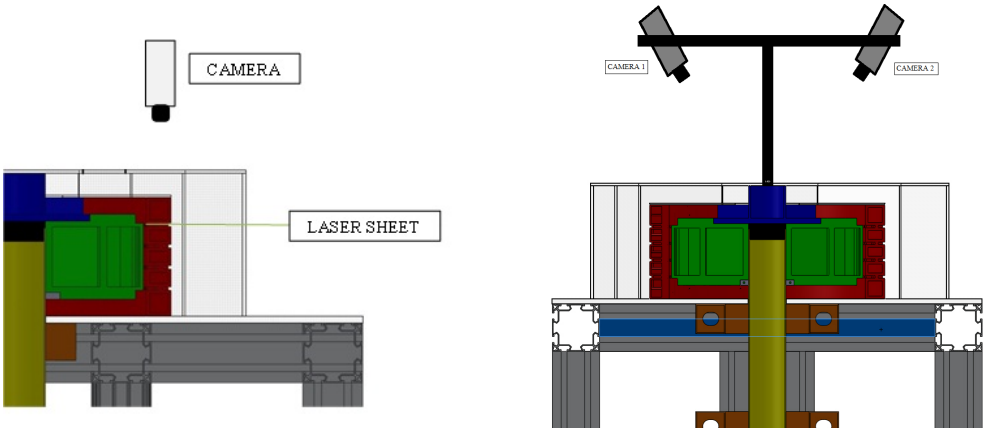

(a) 2D-2C PIV (b) 2D-3C / stereo PIV

Figure 2.2: PIV setup

gions was due to the fact that the air flow is rather different in those two regions. Due to the small stator channel height (4.7mm), it was assumed that the flow in that region was 2D. Outside the stator the flow was assumed to be 3D.

Black painting was done to the stator channel, stator body and rotor body in order to minimize the reflection that was generated by their surfaces. Dummy channels were created for increasing the visibility when measuring row 2 and row 3 of the stator. An external rig was built in order to support the camera and laser arm.

2.1 PIV System Setup

The PIV system that was used in this work consists of :

- DaVis 8.0 PIV software
- Spectra-Physics double-pulsed Nd:YAG laser with 400mJ/pulse energy
- Imager pro X 4M 2048x2048 CCD camera
- Sigma lens 105 mm macro
- Nikon lens 28 mm

The 2D-2C PIV measurements of 4 stator channels was divided into 2 steps. The two uppermost channels were measured from above and two lowermost channels were measured from below. This procedure

had to be done in order to improve the visibility for the camera in order to capture the images in the channels. With this method, the lowermost channel could be measured the same way as the uppermost channel, rather than the camera had to see through 3 stator channels before reaching the lowermost channel.

2D-3C (stereo) PIV measurements were done for the flow outside the stator channel. For the PIV measurement all the measurements were done with the camera at the top of the generator. There was not enough space to do the measurements from below, and there were no advantage for measuring from below.

The schematic view of the setup can be seen in Figure 2.2.

2.2 Transparent Channel Modification

Before modifying the rotor, stator, and channel walls, there were many reflections and light scatterings captured by the camera. These reflections caused problems when post-processing the data. One way to minimize this problem was by painting the surfaces around the measurement region with black colour. The paint that was used was ink from Faber-Castell Multimark 1513 permanent marker. This particular paint was chosen due to its shiny surface finish and very dark black colour. Figure 2.3 show where the paint was applied at the channel walls.

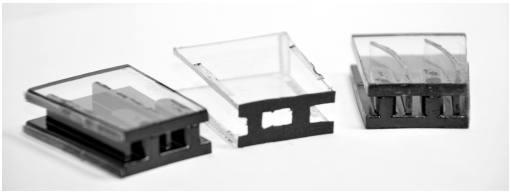

Figure 2.3: Modified transparent channels inserts. From left to right: straight channel, dummy channel, curved channel

Another modification that has been made in order to give better visibility access was to create a dummy channel. A dummy channel is a channel without coils and baffles inside it, but still have the same blockage effect at the inlet using paper that mimics the inlet of the original channel, see Figure 2.3, center. The reason for creating the dummy channel was that there were difficulties in making a fully transparent channel with baffles and coils inside it. This was due to difficulties in attaching the coils and baffles at the correct location, i.e. align with the coils and baffles underneath. The dummy channel was inserted in

the uppermost and lowermost positions while measuring in the center channels

When measuring the straight stator channel, there were no special treatment at the channel, only painted black. For the curved channel there were a special modification besides the black paint. The baffles of the curved stator channel were slightly modified in order to minimize the shadow region that was created by the baffles. The baffles were made from fully transparent material in order to allow laser light to pass through and the baffles tail was modified slightly in order to minimize the shadow area that was created by it. It was made sharp at the end of the tail, rather than flat. Figure 2.4 shows a comparison between un-modified and modified baffles tail.

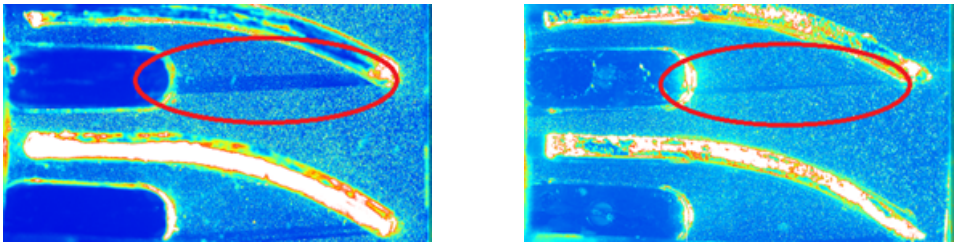

(a) Before modification (b) After modification

Figure 2.4: Modification of the baffle tail

2.3 Seeder

An in-house particle generator was specially built for this work. Before building the in-house particle generator, several attempts to introduce particles into the generator were made but they created problems. Two major problems were that the hot smoke tends to condensate quite quickly and stick to the enclosure wall and reduced visibility and that the smoke that was created could not give a constant supply of particle into the generator.

The particle generator design was based on Kähler et al. (2002). The particle generator that was used in this work was a water filter, see Figure 2.5. The flow direction of the water filter was altered and an extra pipe with 12 tiny nozzles (1 mm in diameter) was attached. The inlet was supplied with high pressure air, approximately 1 bar, depending on the density of the particle that was needed. The high pressure air that came out from the nozzle broke the fog fluid into tiny particles. These tiny particles, approximately 1m, were used as tool to measure the velocity field. Inside the tube a non-toxic fog fluid was

used as a liquid source. The fog fluid filled the tube until all the 12 nozzles were immersed.

The in-house particle generator could give a constant supply of particles into the system and due to its low temperature the smoke did not condensate at the walls. The deposition of particles was found at the enclosure wall after a long time of period, longer than the hot smoke. A drawback was the fog fluid solvent the paint in long run.

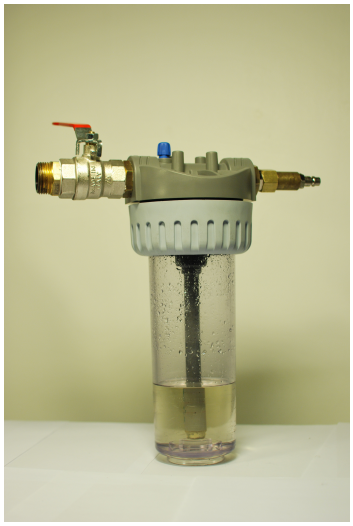

Figure 2.5: In-house particle generator

2.4 External rig

Due to vibration of the generator rig, a new external rig for the PIV system was built. This external rig was mainly built to handle the camera and laser arm. The external rig was equipped with a traverse system so that the distance between the camera and laser plane remained constant. Thus it was not necessary to re-adjust the camera focus every time the measurement points moved.

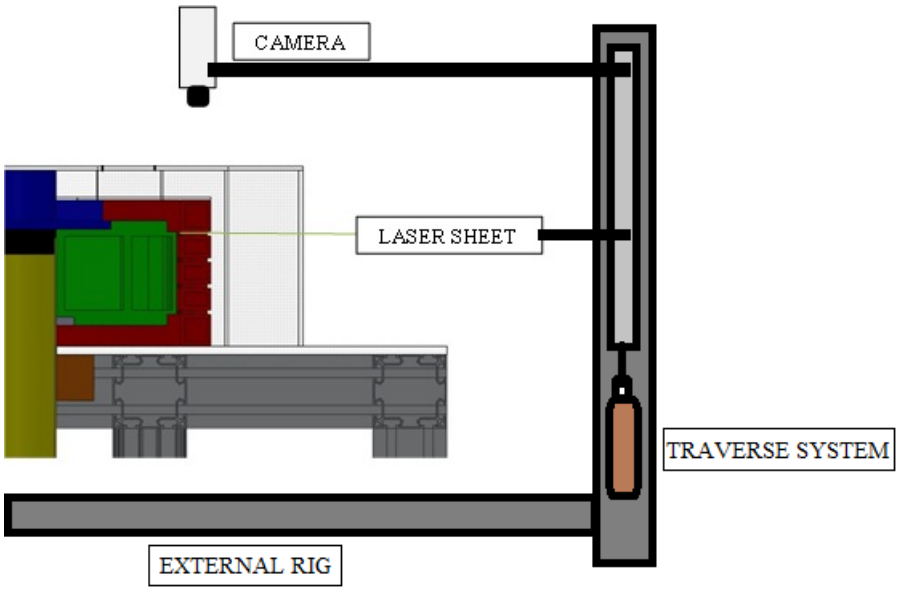

Figure 2.6: External rig for camera and laser arm

Chapter 3

Results and Discussion

In this chapter result from PIV measurement will be shown and discussed. The data from PIV software were post processed by MATLAB.

3.1 Inner region

This region was measured with the 2D-3C stereo PIV technique. The velocity distribution was reconstructed in this region by ”scanning”. Scanning here means capturing the flow layer by layer in the radial-tangential plane and then interpolating the data to get an approximation of the flow in the radial-axial plane. Five layers were used for the scanning of this region.

Figure 3.1 shows the scanned velocity distribution in the inner region. The flow is dominated by the tangential component. Another interesting feature is a region of positive radial velocity. Positive means that the flow goes outwards from the center of rotation. This phenomenon may be due to pressure forces and shear forces unbalance near the entrance. A flow separation has occured here. The axial components near the entrance to the fan has a positive value. This positive value means that the flow is upwards. The flow should have a negative axial velocity in that region since the flow should be downward into the fan.

For the straight stator, the flow is according to intuition. A high tangential component is predicted due to the shaft rotation. Negative radial components indicate the flow is towards the centre of rotation. Negative axial components make the flow go into the fan.

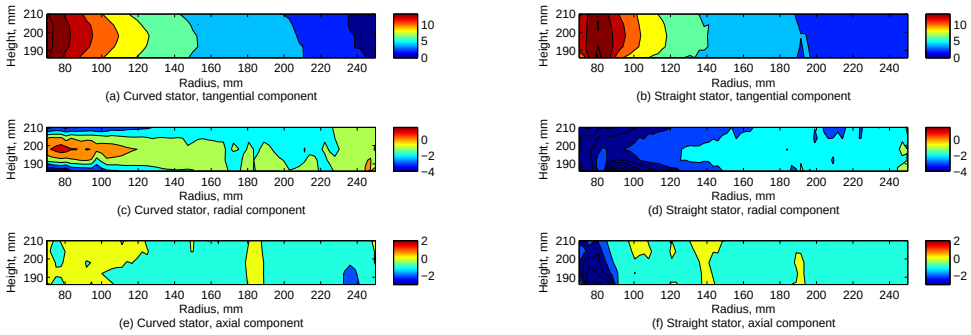

Figure 3.1: Contour plot of velocity components in inner region

3.2 Outer region

The outlet jet from the stator was turned tangentially and deflected upward quite sudden, following the rotation direction of the shaft. In order to capture this behaviour, ”scanning” of the outer region with stereo PIV in 15 layers was done. The velocity contour that is shown in Figure 3.2 is an average of 100 slices circumferentially.

It can be seen that the velocity in the outer region is quite small compared to the velocity in the inner region. The tangential velocity component still dominates the flow. The jets that come out of the stator channels are slightly larger with the curved stator compared to the straight stator. In the stator channel region ($r = 41, 72, 113, 134mm$) the radial velocity component is slightly larger compared to other regions.

3.3 Overview region

The overview region is a combination of the inner and outer regions, see Figure 2.1. With this combination an overview of the flow can be seen, and the flow cycle inside the enclosure can be approximated. Figure 3.3 shows the result of the combination.

Figure 3.3 shows the velocity distribution in the radial-axial plane in the enclosure, from scanning reconstructions. There is a blank white spot at the upper left corner of the contour plot, which is a region that was not covered due to the view angle of the camera. The camera that was used is not wide enough to capture all the region from the centre of rotation to the enclosure side wall. The velocity is taken at the mid-plane of the measurement region. The flow structure does not differ much from the averaged velocity in Figures 3.1 and 3.2. This indicates

that the flow is periodic. The small differences are due to the measurement noise.

3.4 Stator Channels

The previous study by Hartono (2011) concluded that half of the stator channels were consumed by a recirculation region. Moradnia (2010) also numerically estimated that the air flow was recirculating in the stator channels.

Figures 3.4 and 3.5 show the velocity distribution in the stator channels with an emphasis on two cross-sections referred to as ”inlet” and ”outlet”. The vertical lines show the location of the ”inlet” and ”outlet”. The flow in the stator channels is quasi-two-dimensional. At the inlet the radial component dominates the flow. An interesting feature is the negative radial velocity at one side of the coil. This negative radial velocity is due to the adverse pressure gradient. The high tangential velocity in the gap between the rotor and stator creates a low pressure region on the ”backside” of the coil. This low pressure is a driving force that makes the radial velocity become negative. The flow then enters the neighbouring channel. At the outlet, the tangential velocity component is increasing due to the strong swirl outside the stator.

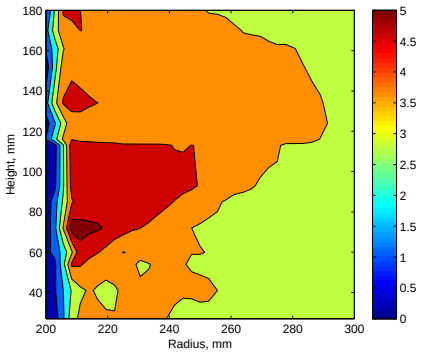

(a) Curved stator, tangential component

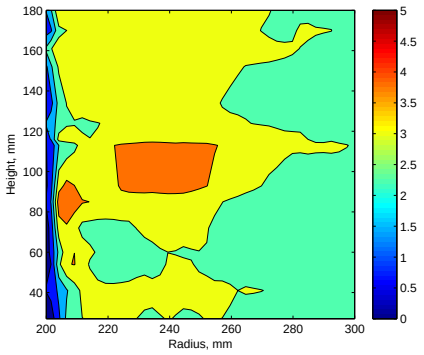

(b) Straight stator, tangential component

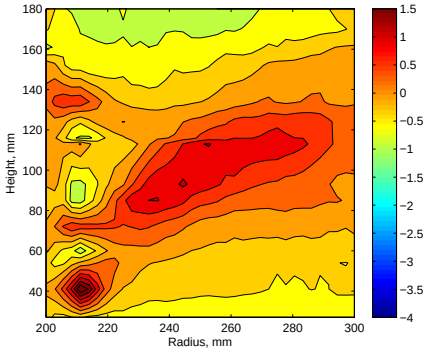

(c) Curved stator, radial component

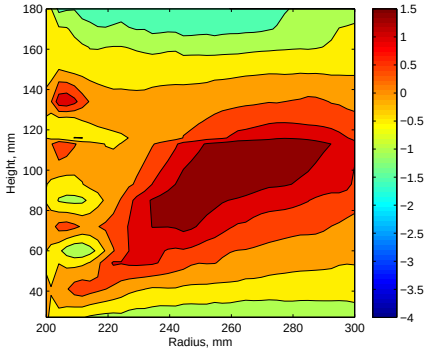

(d) Straight stator, radial component

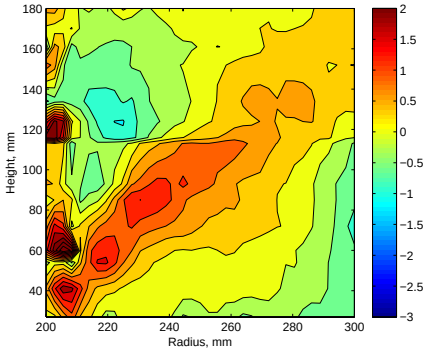

(e) Curved stator, axial component

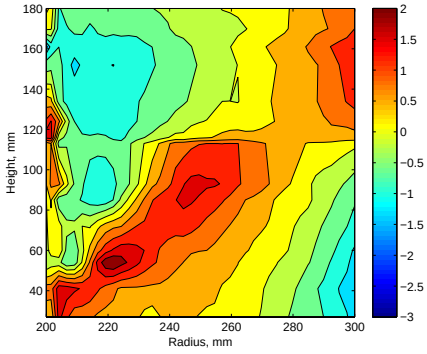

(f) Straight stator, axial component

Figure 3.2: Outer region velocity distribution

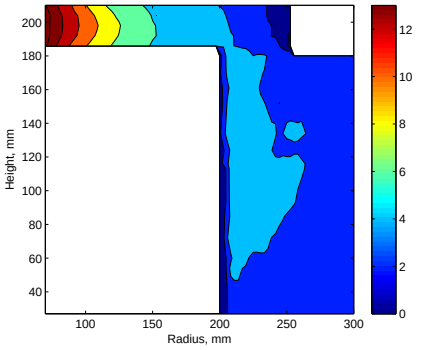

(a) Curved stator; tangential component

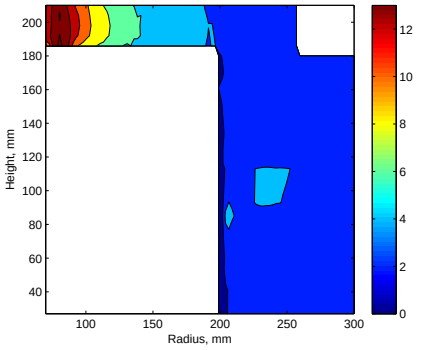

(b) Straight stator; tangential component

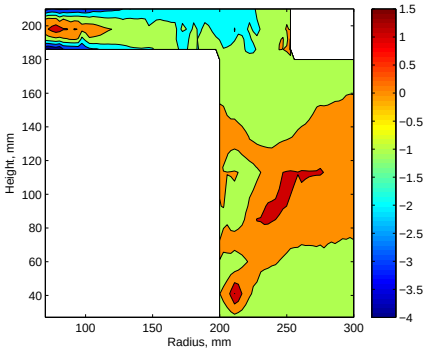

(c) Curved stator; radial component

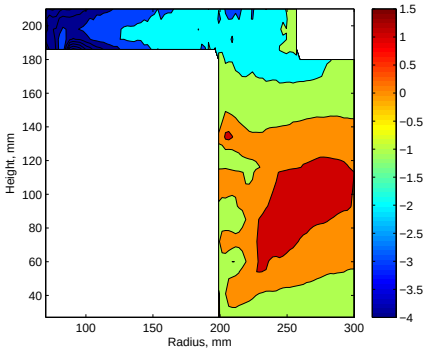

(d) Straight stator; tangential component

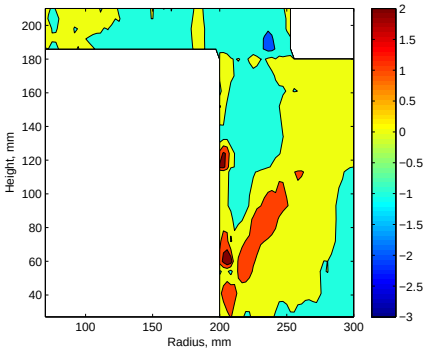

(e) Curved stator; axial component

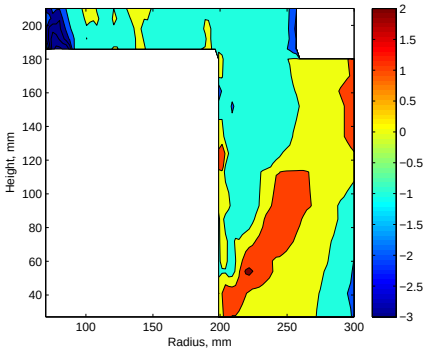

(f) Straight stator; tangential component

Figure 3.3: Overview of the flow inside the enclosure

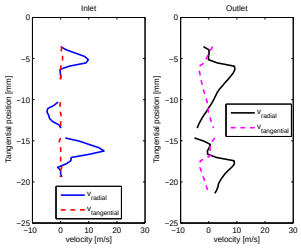

(a) Velocity profile at inlet and outlet at row 1 in curved channel

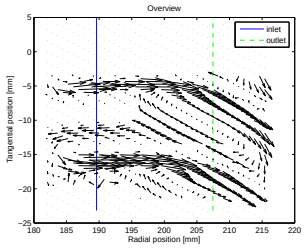

(b) Velocity vector plot at inlet and outlet at row 1 in curved channel

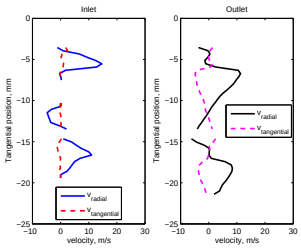

(c) Velocity profile at inlet and outlet at row 2 in curved channel

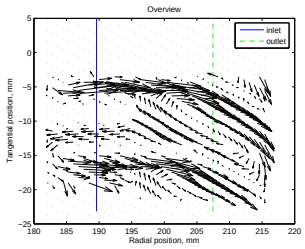

(d) Velocity vector plot at inlet and outlet at row 2 in curved channel

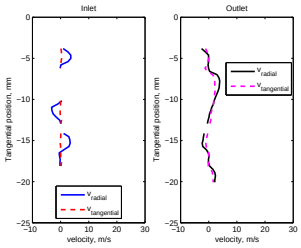

(e) Velocity profile at inlet and outlet at row 3 in curved channel

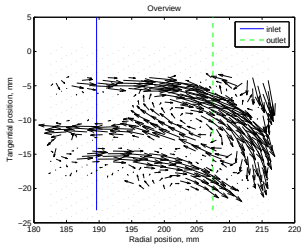

(f) Velocity vector plot at inlet and outlet at row 3 in curved channel

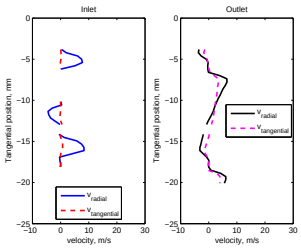

(g) Velocity profile at inlet and outlet at row 4 in curved channel

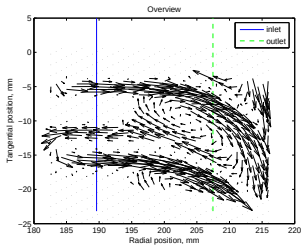

(h) Velocity vector plot at inlet and outlet at row 4 in curved channel

Figure 3.4: Velocity distribution in the curved channel in rows 1(a,b), 2(c,d), 3(e,f), 4(g,h)

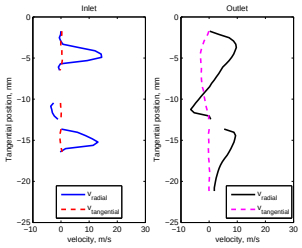

(a) Velocity profile at inlet and outlet at row 1 in straight channel

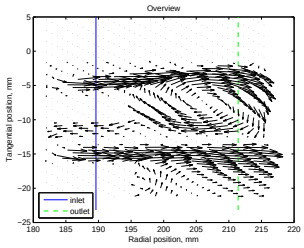

(b) Velocity vector plot at inlet and outlet at row 1 in curved channel

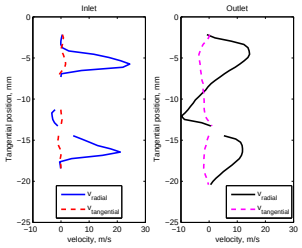

(c) Velocity profile at inlet and outlet at row 2 in curved channel

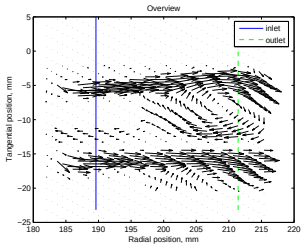

(d) Velocity vector plot at inlet and outlet at row 1 in curved channel

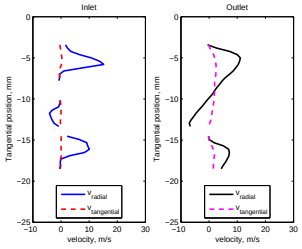

(e) Velocity profile at inlet and outlet at row 3 in curved channel

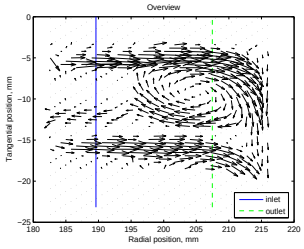

(f) Velocity vector plot at inlet and outlet at row 1 in curved channel

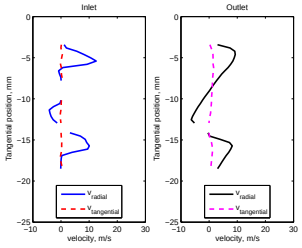

(g) Velocity profile at inlet and outlet at row 4 in curved channel

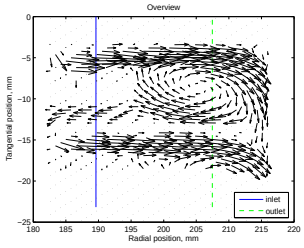

(h) Velocity magnitude vector field

Figure 3.5: Velocity distribution in the straight channel in rows 1(a,b), 2(c,d), 3(e,f), 4(g,h)

Chapter 4

Conclusion and Future Work

4.1 Conclusion

This work studied the cooling air flow inside the model of an electric generator, with PIV. The model is based on an existing generator at Uppsala University, with some modifications in order to fulfil the requirement of optical access and to simplify the numerical simulations. Two configurations of stator channel baffles, straight and curved, were studied.

Inside the stator channels, 2D-2C PIV was used to measure velocity field. 2D-3C PIV was used to measure the other region, such as the region between the stator top lid and the top enclosure wall, and the region between the stator and the enclosure side wall.

Laser measurements need surfaces that do not reflect too much light. Ideally there are only two options to get the best PIV results, either fully transparent or fully black surfaces. In the present work, all surfaces that were not required to be transparent were painted black.

The results of the present work verify the predictions from the numerical studies and the results from pressure measurements. There are recirculations inside the channels, which consume half of the channel width. This phenomenon occurred both for the straight and curved stator channel configurations.

Outside the stator the flow is highly three-dimensional and has a strong swirl. The velocity field shows that the flow rotates around the shaft with the same rotational direction as the shaft. The highest tangential velocity occurs near the shaft and the velocity decreases further away from the shaft, as a free vortex.

4.2 Future Work and Recommendation

With water instead of air, a higher Reynolds number can be achieved with the same rotational speed, which is more beneficial for PIV. It also reduces the light refraction due to similar optical properties of water and plexi-glass.

A torque meter can be added to measure the torque that is used to rotate the rotor, fan, shaft, and air. With this modification the windage losses can be estimated.

A new method should be considered in order to minimize the error due to misalignment of the insertion of the transparent channels. From experience, small misalignments of the insertion gave large changes in the velocity field data.

Appendices

Appendix A

Velocity plot of inner and outer region

A.1 Line plot per layer of inner region

In section 3, the experimental data in the inner region was presented as contour plots. The contour plots were made from interpolations between the different layers of the measurements. Figure A.1 shows the data used in that interpolation. The tangential velocity at the shaft is the same as that of the shaft according to

$$\begin{aligned} V_{tan,shaft} &= \omega r \\ V_{tan,shaft} &= \frac{2\pi}{60} Nr \\ V_{tan,shaft} &= \frac{2\pi}{60}(2000)(0.035) \\ V_{tan,shaft} &= 7.33\ m/s \end{aligned} \tag{A.1}$$

The presence of fan blades increase the tangential velocity along the fan inlet. This is the reason why the velocity is increasing with radius, at small radii. The fan blade tangential velocity at the outer part of the inlet is given by

$$\begin{aligned} V_{tan,shaft} &= \omega r \\ V_{tan,shaft} &= \frac{2\pi}{60} Nr \\ V_{tan,shaft} &= \frac{2\pi}{60}(2000)(0.060) \\ V_{tan,shaft} &= 12.56\ m/s \end{aligned} \tag{A.2}$$

Further away from the fan inlet the tangential velocity reduces and approaches zero at the enclosure side wall.

Data from measurement contain some noises due to reflection. In post processing the data was made smooth by the method of local regression using weighted linear least squares and a 2nd degree polynomial model. The smoothen data is shown with dashed line in figure A.1.

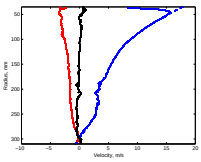

(a) Curved stator; $Z = 210\ mm$

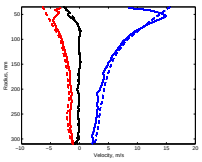

(b) Straight stator; $Z = 210\ mm$

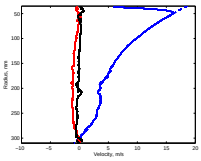

(c) Curved stator; $Z = 204\ mm$

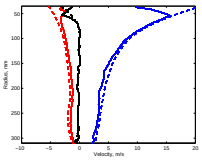

(d) Straight stator; $Z = 204\ mm$

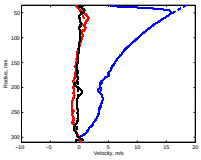

(e) Curved stator; $Z = 198\ mm$

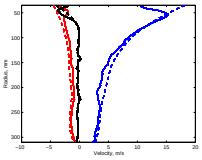

(f) Straight stator; $Z = 198\ mm$

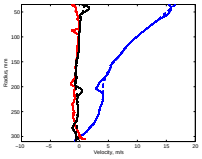

(g) Curved stator; $Z = 192\ mm$

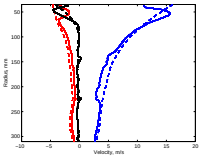

(h) Straight stator; $Z = 192\ mm$

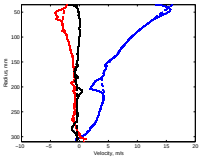

(i) Curved stator; $Z = 186\ mm$

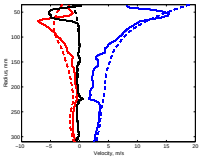

(j) Straight stator; $Z = 186\ mm$

Figure A.1: Velocity distribution along radial lines at different heights above the stator lid

A.2 Line plot per layer of outer region

In section 3, the experimental data in the outer region was presented by contour plots. The contour plots were made from interpolations between the different layers of the measurements. Figure A.4 shows the data used in that interpolation.

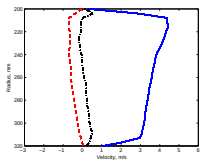

(a) Curved stator; $Z = 180\ mm$

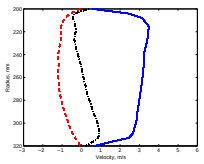

(b) Straight stator; $Z = 180\ mm$

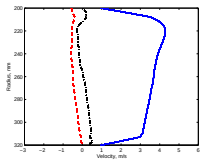

(c) Curved stator; $Z = 170\ mm$

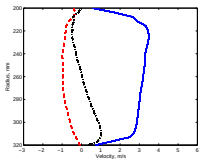

(d) Straight stator; $Z = 170\ mm$

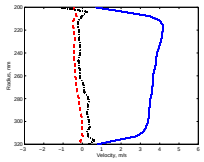

(e) Curved stator; $Z = 161\ mm$

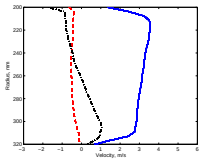

(f) Straight stator; $Z = 161\ mm$

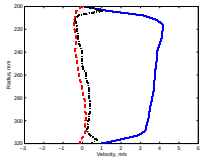

(g) Curved stator; $Z = 152\ mm$

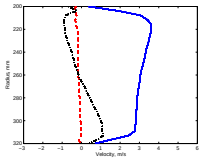

(h) Straight stator; $Z = 152\ mm$

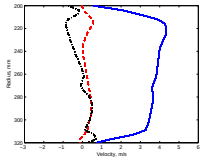

(i) Curved stator; $Z = 134\ mm$

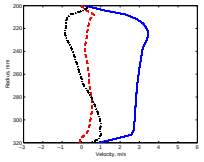

(j) Straight stator; $Z = 134\ mm$

Figure A.2: The Average velocity at outer region in different layer in axial direction

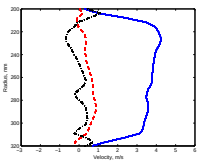

(a) Curved stator; $Z = 124\ mm$

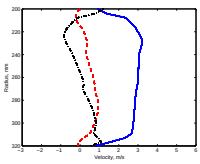

(b) Straight stator; $Z = 124\ mm$

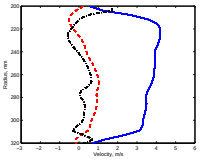

(c) Curved stator; $Z = 116\ mm$

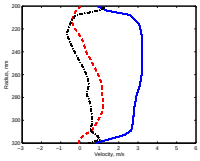

(d) Straight stator; $Z = 116\ mm$

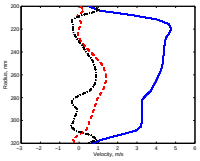

(e) Curved stator; $Z = 113\ mm$

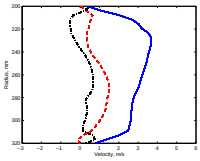

(f) Straight stator; $Z = 113\ mm$

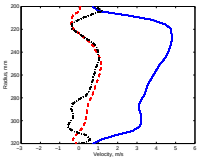

(g) Curved stator; $Z = 93\ mm$

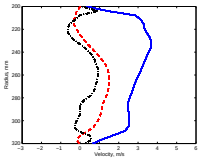

(h) Straight stator; $Z = 93\ mm$

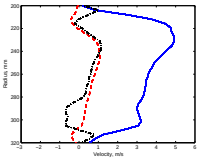

(i) Curved stator; $Z = 85\ mm$

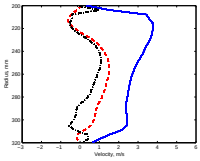

(j) Straight stator; $Z = 85\ mm$

Figure A.3: The Average velocity at outer region in different layer in axial direction

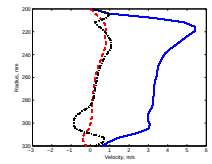

(a) Curved stator; $Z = 72\ mm$

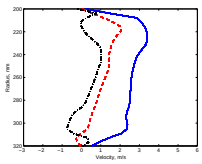

(b) Straight stator; $Z = 72\ mm$

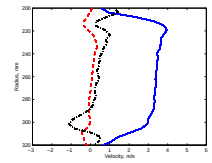

(c) Curved stator; $Z = 60\ mm$

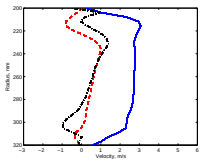

(d) Straight stator; $Z = 60\ mm$

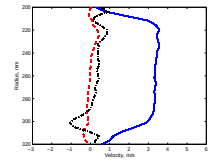

(e) Curved stator; $Z = 54\ mm$

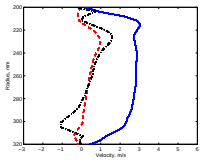

(f) Straight stator; $Z = 54\ mm$

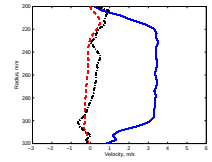

(g) Curved stator; $Z = 41\ mm$

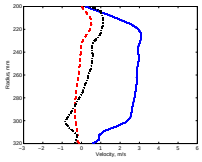

(h) Straight stator; $Z = 41\ mm$

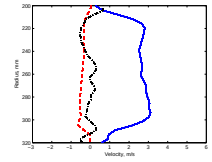

(i) Curved stator; $Z = 27\ mm$

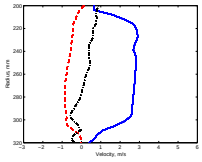

(j) Straight stator; $Z = 27\ mm$

Figure A.4: The Average velocity at outer region in different layer in axial direction

Appendix B

PIV Software Setup

After obtaining all the pictures from the PIV recording, a set of software parameters have to be set to post-process the raw data. This post process transforms the pictures into velocity vector fields. It is based on the displacement of the particles between two images.

In this work the majority of the parameters were set the same for 2D-2C and 2D-3C PIV. The only difference was that for 2D-2C, cross correlation was used as vector calculation parameter, and for 2D-3C, stereo cross-correlation was used.

Operation list

- PIV
  - group : vector calculation - double frames
  - operation : PIV
- Vector Calculation Parameter
  - stereo cross correlation (for 2D-3C PIV) or Cross Correlation (for 2D-2C PIV)
  - iterations : multi pass
  - Window size and weight

    64×64 $1:1$ Overlap 25% passes = 2
    32×32 $1:1$ Overlap 25% passes = 2
- Multipass option
  - Initial window shift for image reconstruction (first pass only) = constant
  - Correlation function

    All initial passes 'standard'I1*I2 (via FFT, no zero padding)
    Final passes 'standard'I1*I2 (via FFT, no zero padding)

  - Derformed integration windows = symmetric shift (both frames)
  - 3D vector validation = accept (V_x, V_y, V_z) if stereo reconstruction error < 5 pixel

- Multi pass post processing

  Delete vector if its peak ratio $Q < 1.3$
  $1 \times$ median filter strongly remove iteratively replace
  remove if diff. to avg. > 2 *rms of neighbours
  reinsert if diff. to avg. < 3 *rms of neighbours
  smoothing 1 $\times$ smooth 3×3

- Vector post processing

  Delete vector if its peak ratio $Q < 1.5$
  $1\times$ median filter strongly remove iteratively replace
  remove if diff. to avg. > 2 *rms of neighbours
  reinsert if diff. to avg. < 3 *rms of neighbours
  remove groups with < 9 vectors
  fill up empty spaces (interpolation)
  fill up all smoothing $1\times$ smooth 3×3

Bibliography

[1] J. Anthonie et al., "Measurement Techniques in Fluid Dynamics; An Introduction", 3^{rd} revised edition, Ed. by T. Arts, The Von Karman Institute, 2009.

[2] M. Fujita et al., "Air-Cooled Large Turbine Generator with Multiple-Pitched Ventilation Ducts", IEEE, pp. 910-912, 2005.

[3] B. Lidell et al., "Redesigning The Rotor Fan Blades to Improve the Cooling of Roxburgh's Hydro-Generators", 14^{th} Australian Fluid Mechanics Conference, Adelaide University, Adelaide, Australia, pp. 465-468, 2001.

[4] P. Moradnia, V. Chernoray, H. Nilsson., "Experimental and Numerical Investigation of The Cooling Air Flow in An Electric Generator", 8^{th} International Conference on Heat Transfer, Fluid Mechanics, and Thermodynamics, 2011.

[5] P. Moradnia and H. Nilsson., "CFD of Air Flow in Hydro Power Generator for Convective Cooling Using OpenFOAM", V European Conference on Computational Fluid Dynamics. Ed. by. J. Pereira and A. Sequeria., ECCOMAS CFD 2010, Lisbon, Portugal, 2010.

[6] P. Moradnia., "CFD of Air Flow in Hydro Power Generator", Licentiate Thesis. Chalmers University of Technology, Göteborg, Sweden. 2010.

[7] N.J. Carew., "Flow Distribution and Pressure Drop In Salient Pole Electrical Machines", Proc Instn Mech Engrs 184 pt 3E.8(1969-1970), pp. 62-69.

[8] N.J. Carew and D. Freeston., "Fluid Flow Losses in A.C. Generator Stator Ventilating Ducts", Proc Instn Mech Engrs 182.12 (1967-1968), pp. 87-95.

[9] D. Shuye et al., "Research of Fluid Flow Characteristic Inside Radial Ventilation Ducts for Large Generator", IEEE 10.978-1-4244-4813-5, 2010.

[10] K. Toussaint et al., "CFD Analysis of Ventilation Flow for a Scale Model Hydro-Generator", Proceeding of the ASME 2011 Power Conference. Vol. POWER2011-55202, Denver, Colorado, USA, 2011.

[11] C.J. Kähler, B. Sammler, J. Kompenhams., "Generation and Control of Tracer Particles for Optical Flow Investigations in Air", Exp. in Fluids 33:736-742, 2002.

[12] E.A. Hartono., "Experimental Study of Air Flow in a Hydro Power Generator Model, Design, Construction, and Measurements", Master Thesis 2011:51, Chalmers University of Technology, Sweden, 2011.

[13] M. Jahanmiri., "Particle Image Velocimetry: Fundamentals and its Application", Research Report 2011:3, Chalmers University of Technology, Sweden, 2011.

[14] R.L. Panton., "Incompressible Flow", 3^{rd} edition, John Wiley & sons, Canada, 2005